Research Article | Vol. 26, No. 4 | 19 Feb 2018 | OPTICS EXPRESS 4674
Optics EXPRESS

Fast recognition of single quantum dots from high multi-exciton emission and clustering effects

BIN LI,[1,2] GUOFENG ZHANG,[1,2,4] CHANGGANG YANG,[1,2] ZHIJIE LI,[1,2] RUIYUN CHEN,[1,2] CHENGBING QIN,[1,2] YAN GAO,[1,2] HE HUANG,[3] LIANTUAN XIAO,[1,2,5] AND SUOTANG JIA[1,2]

[1]*State Key Laboratory of Quantum Optics and Quantum Optics Devices, Institute of Laser Spectroscopy, Shanxi University, Taiyuan, 030006, China*
[2]*Collaborative Innovation Center of Extreme Optics, Shanxi University, Taiyuan, Shanxi, 030006, China*
[3]*Department of Materials Science and Engineering, Centre for Functional Photonics (CFP), City University of Hong Kong, 83 Tat Chee Avenue, Kowloon, Hong Kong*
[4]*guofeng.zhang@sxu.edu.cn*
[5]*xlt@sxu.edu.cn*

Abstract: Recognition of single quantum dots (QDs) from high multi-exciton emission and clustering effects is challenging using the conventional second-order correlation function method. Here we demonstrate a method for fast recognizing single QDs based on the probabilities of detecting single- and two-photon events. The time-tagged, time-resolved and time-correlated single-photon counting technique is applied to effectively remove multi-exciton emission and low-counting background. By this way, single QDs can be fastly recognized by the spatial coincidence-counting model. In addition, the fast recognition of single QDs by using the collected photons during the confocal scanning imaging process has been achieved synchronously.

OCIS codes: (300.6500) Spectroscopy, time-resolved; (300.2530) Fluorescence, laser-induced; (160.4236) Nanomaterials.

References and links

1. L. Su, H. F. Yuan, G. Lu, S. Rocha, M. Orrit, J. Hofkens, and H. Uji-I, "Super-resolution localization and defocused fluorescence microscopy on resonantly coupled single-molecule, single-nanorod hybrids," ACS Nano **10**(2), 2455–2466 (2016).
2. G. Zhang, L. Xiao, F. Zhang, X. Wang, and S. Jia, "Single molecules reorientation reveals the dynamics of polymer glasses surface," Phys. Chem. Chem. Phys. **12**(10), 2308–2312 (2010).
3. M. Orrit, T. Ha, and V. Sandoghdar, "Single-molecule optical spectroscopy," Chem. Soc. Rev. **43**(4), 973–976 (2014).
4. Z. Ristanovic, A. V. Kubarev, J. Hofkens, M. B. J. Roeffaers, and B. M. Weckhuysen, "Single molecule nanospectroscopy visualizes proton-transfer processes within a zeolite crystal," J. Am. Chem. Soc. **138**(41), 13586–13596 (2016).
5. H. F. Yuan, S. Khatua, P. Zijlstra, M. Yorulmaz, and M. Orrit, "Thousand-fold enhancement of single-molecule fluorescence near a single gold nanorod," Angew. Chem. Int. Ed. **52**(4), 1217–1221 (2013).
6. B. Li, G. F. Zhang, M. Y. Jing, R. Y. Chen, C. B. Qin, Y. Gao, L. T. Xiao, and S. T. Jia, "Single molecule optical-probes measured power law distribution of polymer dynamics," Acta Phys. Sin.-ch. ed. 65, 218201 (2016).
7. Y. C. Chen, P. S. Salter, S. Knauer, L. Y. Weng, A. C. Frangeskou, C. J. Stephen, S. N. Ishmael, P. R. Dolan, S. Johnson, B. L. Green, G. W. Morley, M. E. Newton, J. G. Rarity, M. J. Booth, and J. M. Smith, "Laser writing of coherent colour centres in diamond," Nat. Photonics **11**(2), 77–80 (2017).
8. T. Hensgens, T. Fujita, L. Janssen, X. Li, C. J. Van Diepen, C. Reichl, W. Wegscheider, S. Das Sarma, and L. M. K. Vandersypen, "Quantum simulation of a Fermi-Hubbard model using a semiconductor quantum dot array," Nature **548**(7665), 70–73 (2017).
9. Y. Y. Fan, H. L. Liu, R. C. Han, L. Huang, H. Shi, Y. L. Sha, and Y. Q. Jiang, "Extremely high brightness from polymer-encapsulated quantum dots for two-photon cellular and deep-tissue imaging," Sci. Rep. **5**(1), 9908 (2015).

#318810 https://doi.org/10.1364/OE.26.004674
Journal © 2018 Received 2 Jan 2018; revised 5 Feb 2018; accepted 7 Feb 2018; published 13 Feb 2018

Optics EXPRESS

10. B. Li, G. F. Zhang, Z. Wang, Z. J. Li, R. Y. Chen, C. B. Qin, Y. Gao, L. T. Xiao, and S. T. Jia, "Suppressing the fluorescence blinking of single quantum dots encased in N-type semiconductor nanoparticles," Sci. Rep. **6**(1), 32662 (2016).
11. Z. Li, G. Zhang, B. Li, R. Chen, C. Qin, Y. Gao, L. Xiao, and S. Jia, "Enhanced biexciton emission from single quantum dots encased in N-type semiconductor nanoparticles," Appl. Phys. Lett. **111**(15), 153106 (2017).
12. X. D. Ma, O. Roslyak, J. G. Duque, X. Y. Pang, S. K. Doorn, A. Piryatinski, D. H. Dunlap, and H. Htoon, "Influences of exciton diffusion and exciton-exciton annihilation on photon emission statistics of carbon nanotubes," Phys. Rev. Lett. **115**(1), 017401 (2015).
13. Y. M. He, G. Clark, J. R. Schaibley, Y. He, M. C. Chen, Y. J. Wei, X. Ding, Q. Zhang, W. Yao, X. Xu, C. Y. Lu, and J. W. Pan, "Single quantum emitters in monolayer semiconductors," Nat. Nanotechnol. **10**(6), 497–502 (2015).
14. F. R. Hu, B. H. Lv, C. Y. Yin, C. F. Zhang, X. Y. Wang, B. Lounis, and M. Xiao, "Carrier multiplication in a single semiconductor nanocrystal," Phys. Rev. Lett. **116**(10), 106404 (2016).
15. V. I. Klimov, A. A. Mikhailovsky, S. Xu, A. Malko, J. A. Hollingsworth, C. A. Leatherdale, H. J. Eisler, and M. G. Bawendi, "Optical gain and stimulated emission in nanocrystal quantum dots," Science **290**(5490), 314–317 (2000).
16. T. Heindel, A. Thoma, M. von Helversen, M. Schmidt, A. Schlehahn, M. Gschrey, P. Schnauber, J. H. Schulze, A. Strittmatter, J. Beyer, S. Rodt, A. Carmele, A. Knorr, and S. Reitzenstein, "A bright triggered twin-photon source in the solid state," Nat. Commun. **8**, 14870 (2017).
17. F. T. Rabouw, R. Vaxenburg, A. A. Bakulin, R. J. A. van Dijk-Moes, H. J. Bakker, A. Rodina, E. Lifshitz, A. L. Efros, A. F. Koenderink, and D. Vanmaekelbergh, "Dynamics of intraband and interband auger processes in colloidal core-shell quantum dots," ACS Nano **9**(10), 10366–10376 (2015).
18. N. Hiroshige, T. Ihara, and Y. Kanemitsu, "Simultaneously measured photoluminescence lifetime and quantum yield of two-photon cascade emission on single CdSe/ZnS nanocrystals," Phys. Rev. B **95**(24), 245307 (2017).
19. N. Mishra, N. J. Orfield, F. Wang, Z. Hu, S. Krishnamurthy, A. V. Malko, J. L. Casson, H. Htoon, M. Sykora, and J. A. Hollingsworth, "Using shape to turn off blinking for two-colour multiexciton emission in CdSe/CdS tetrapods," Nat. Commun. **8**, 15083 (2017).
20. Y. J. Choi, D. Hwang, H. Chung, D. Y. Kim, and D. Kim, "Controlling the spatial distribution of quantum dots in nanofiber for light-harvesting devices," NPG Asia Mater. **7**(7), e202 (2015).
21. B. D. Mangum, Y. Ghosh, J. A. Hollingsworth, and H. Htoon, "Disentangling the effects of clustering and multi-exciton emission in second-order photon correlation experiments," Opt. Express **21**(6), 7419–7426 (2013).
22. S. L. Dong, T. Huang, Y. Liu, J. Wang, G. F. Zhang, L. T. Xiao, and S. T. Jia, "Fast recognition of single molecules based on single-event photon statistics," Phys. Rev. A **76**(6), 063820 (2007).
23. H. Ta, J. Keller, M. Haltmeier, S. K. Saka, J. Schmied, F. Opazo, P. Tinnefeld, A. Munk, and S. W. Hell, "Mapping molecules in scanning far-field fluorescence nanoscopy," Nat. Commun. **6**(1), 7977 (2015).
24. X. Brokmann, G. Messin, P. Desbiolles, E. Giacobino, M. Dahan, and J. P. Hermier, "Colloidal CdSe/ZnS quantum dots as single-photon sources," New J. Phys. **6**, 99 (2004).

1. Introduction

Recognition of single particles is absolutely critical for the studies on single-molecule spectroscopy of nanoscale light emitters such as dye molecules [1–6], colour centres [7], quantum dots (QDs) [8–11], carbon nanotubes [12], and defects in two-dimensional materials [13]. The second-order correlation function, $g^{(2)}(\tau)$, is generally used to recognize single particles from their clusters based on the photon anti-bunching effect. Recently, single particles with biexciton (BX) quantum yields approaching unity have been developed for the applications in carrier multiplication [14], light amplification [15] and photon pair sources [16]. For these QDs, the peak of the $g^{(2)}(\tau)$ at zero-time delay becomes significant due to the emission of two-photon from BX states. Therefore, it is challenging to recognize such single QDs due to high BX emission and clustering effects when the BX emission is not spectrally excluded in the $g^{(2)}(\tau)$ measurement. Recently, insight into the essential characteristics of the multi-exciton emission has also been conducted at single-dot level, reporting the dynamics of BX Auger recombination [17], the enhancement of BX emission [11], the quantum yield of two-photon cascade emission [18], the two-colour multi-exciton emission [19] and so on. Nonetheless, the colloidal QDs is susceptible to aggregation in most solvents to form QD clusters [20], making many questions still elusive. Therefore, fast recognition of single QDs with high multi-exciton emission from their clusters prior to single-dot studies becomes increasingly critical for further in-depth investigation at the single-dot level.

Htoon *et al.* have demonstrated a time-gated antibunching approach for recognizing the single QDs with high multi-exciton emission from their clusters [21]. The time-gating method

Optics EXPRESS

effectively removes the photons caused by BX emission based on the shorter BX lifetimes than that of single exciton (SX) states, and then reconstruct the $g^{(2)}(\tau)$ to discriminate single QDs from QD clusters. As discussing the recognition of single particles, it is worth mentioning the recognition methods of single dye molecules. In our previous work, we have demonstrated a method to fastly recognize single dye molecules based on the Mandel's Q parameter of single-event photon statistics, providing an alternative way other than $g^{(2)}(\tau)$ to recognize single dye molecules [22]. Recently, Haisen *et al.* used a spatial coincidence-counting model to recognize the number of single dye molecules [23]. It is based on the characteristics of dye molecules that a single molecule emits only one photon per excitation pulse, and all of the single molecules in the clusters have the same fluorescence brightness and the stable photon emission. However, single QDs are unlike single dye molecules. QDs generally have the high multi-exciton quantum yield and/or the large photoluminescence (PL) blinking. Therefore, the method of the spatial coincidence-counting model is not suitable to directly recognize single QDs nor their number in the cluster.

Here, we apply the time-tagged, time-resolved and time-correlated single-photon counting (TTTR-TCSPC) technique to effectively remove the multi-exciton emission and the low-counting background. By this way, we make QDs' PL photons suitable to the spatial coincidence-counting model. Therefore, single QDs can be recognized based on the probabilities of detecting the single- and two-photon events after individual excitation pulses. In addition, we achieve synchronously the fast recognition of single QDs by using the collected photons during the confocal scanning imaging process.

2. Spatial coincidence-counting model

The coincidence counting is the detection of two or more photons at separate detectors within a short interval of time. In coincidence counting, the single- or two-photon events are defined as detecting one or two photons per excitation pulse, respectively, as shown in Fig. 1(a). In contrast to the conventional coincidence analysis that is based on pulsed laser excitation and direct measurement of coincident photon pairs using a time-to-amplitude converter [24], our method relies on the photon arrival time intervals by recording the absolute arrival time of each PL photon with picosecond time resolution on two single detectors with a 50/50 beam splitter (see Appendix A for experimental details).

In order to recognize the number n of emitters in their clusters based on the spatial coincidence-counting model, the following three assumptions must be satisfied. Assumption-I, an emitter emits only one photon after an excitation pulse. Assumption-II, all emitters in a cluster share the same brightness and their fluorescence emission properties do not depend on each other. Assumption-III, each emitter in the cluster has the stable photon emission. Then the probabilities of single- and two-photon detection events per excitation pulse, denoted with f_1 and f_2, respectively, originating from the cluster with n emitters, can be expressed as [23]:

$$\begin{aligned} f_1 &= nph(r-s)\left[1-ph(r-s)\right]^{n-1} \\ f_2 &= \beta C(n,2)[ph(r-s)]^2\left[1-ph(r-s)\right]^{n-2} \end{aligned} \tag{1}$$

where $ph(r\text{-}s)$ is the probability of detecting a photon from a single emitter located at spatial position s by one excitation pulse. It is mainly determined by three factors: the excitation intensity, the detection efficiency of the confocal microscope, and the properties of the emitters. The properties of emitters include absorption cross-section, fluorescence quantum yield, and dipole moment orientation. $h(r\text{-}s)$ is the point-spread function of the imaging system with r as the coordinate (r is the spatial position of laser excitation). $C(n,2)$ is number of 2-combinations from a given set of n emitters. Moreover, it should be noticed that the two-photon events going through the 50/50 beam splitter may reach the same detector, and thus the information of the photons is partially lost. This loss can be taken into account by

Optics EXPRESS

a geometrical factor $\beta = 1/2$. The value of $[1-ph(r-s)]^n$ is approximately 1 for our confocal microscope due to $ph(r-s) \approx 0.015$. Then, the number of single emitters in the cluster n can be calculated by

$$n = \frac{f_1^2}{f_1^2 - 4f_2}. \tag{2}$$

The number of single emitters n is determined by the values of f_1 and f_2 as shown in Fig. 1(b). For example, n = 1 denoted by the green line means there are no two-photon events and therefore f_2 = 0. The red, blue and pink lines represent n = 2, 3, and 4, respectively. In experiments, the calculated results of n are not always an integer because of background noise. By reducing the background noise, the calculated values of n can become more accurate and further approach to be the integer.

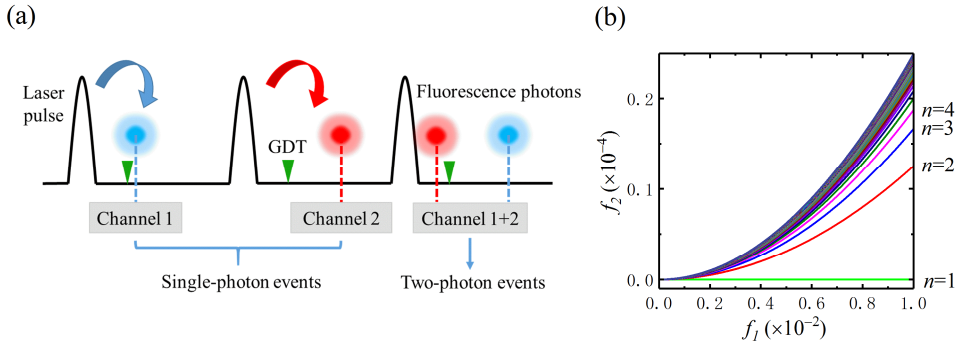

Fig. 1. Schematic of photon-counting measurement and theoretical calculation of the number of emitters n. (a) Schematic for single-photon events and two-photon events. The red and blue circular points represent photons detected by two detectors, respectively. GDT is gate delay time with respect to the laser pulses. (b) The number n of single emitters calculated by the probabilities of single- and two-photon detection events, f_1 and f_2, based on the spatial coincidence-counting model.

If the three assumptions mentioned above are met simultaneously, the number n of single emitters can be calculated correctly by Eq. (2). It is possible to distinguish the number of the emitters up to ~20 by using four single-photon detectors [23]. If the assumption-I is met and the others are not met, the number n cannot be calculated correctly but the single emitters still can be recognized from the cluster. For example, if the emitters have PL blinking which means the fluorescence intensity randomly switching between bright states and dark states, therefore the assumption-II and III are not met. The number of emitters in a cluster staying at bright states changes with time due to blinking. As a result, the calculated number n also changes with time thus cannot give a definite value. If there is only one QD, the number n can be calculated to be approximately 1 by photons from the bright states at any time.

3. Removing the effect of multi-exciton on recognition of single QDs

In the section, we test our method with CdSe/ZnS alloyed QDs which possess both high multi-exciton emission and PL blinking. For the QDs, the assumption-I of the spatial coincidence-counting model does not hold. To solve this problem, fluorescence photons of QDs are modified by the following method. As shown in Fig. 1(a), a suitable time-gating can be used to remove the multi-exciton photons with shorter arrival times from all of the detected photons based on the fact that the lifetimes of multi-exciton are shorter than that of SX [10]. Figure 2(a) displays a typical PL decay curve of single CdSe/ZnS alloyed QDs fitted by a triexponential function with time constants of 8.6 ns, 2.2 ns, and ~0.1 ns. The three-lifetime components are attributed to the relaxations of SX state, trion state and multi-exciton

Optics EXPRESS

state [13,14]. In addition, the lifetime of multi-exciton can be obtained by using first-photon decay analysis [18]. In QDs, the first photon (the multi-exciton photon) stems from the transition from multi-exciton state to SX state, and the second photon (the SX photon) stems from the transition from SX state to ground state [14]. Figure 2(b) displays a typical PL decay curve of the first photons extracted from the two-photon events. The decay curve can be well fitted by a monoexponential function with a time constant of ~0.1 ns. From the decay curve, it is found that the multi-exciton photons almost decay to 0 after 8 ns. Therefore, the gate delay time (GDT) of 8 ns can be set to exclude the multi-exciton photons. In addition, we suppress the impact of shot noise by removing the low-counting state caused by PL blinking (see the Appendix B for details), which can improve the recognition accuracy of single QDs. Moreover, by removing the effects of background counts, dark counts and cross-talk between detectors, f_1 and f_2 are calculated by using the modified fluorescence photons (see the Appendix C for details). Finally, the number n of emitters can be calculated with the f_1 and f_2 by Eq. (2). The calculated number n of emitters as a function of GDT is shown in Fig. 2(c). With GDT of 0 ns, the calculated n of 2.4 implies that the particle is emitting from multi-excitonic states. It is shown that the multi-exciton photons start to be removed at GDT of 2.4 ns. When the GDT is changed from 2.4 ns to 10 ns, the multi-exciton photons are gradually removed and the values of n gradually reduce and finally approach 1, which indicates there is only one single QD in laser focus. The relationship between the first-photon emission and the calculated n is discussed in Appendix F. Finally, we assess the viability of our method by the time-gated antibunching technique (see Appendix D for details). The discussion about lifetime distribution and the recognition with a repetition rate of 5 MHz is shown in Appendix E.

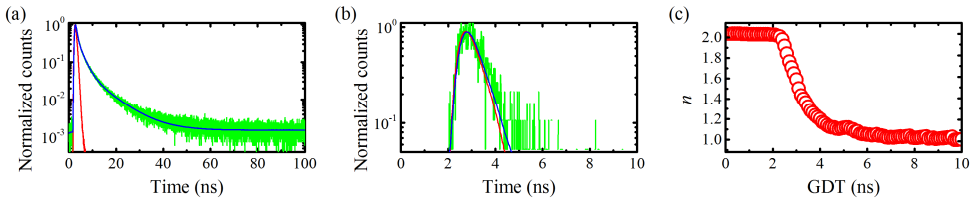

Fig. 2. (a) Typical PL decay curve (green) of single CdSe/ZnS alloyed QDs, and the corresponding fitting curve (blue). The red line is the instrument response function of the system. (b) Typical first-photon decay curve (green) extracted from the two-photon detection events, and the corresponding monoexponential fitting curve (blue). (c) The calculated number n of emitters as a function of GDT and the values of n gradually approach 1 with the increasing GDT.

4. Fast-recognition of single QDs during confocal imaging

In the section, we use this method to recognize the single QDs by using the collected photons during the scanning confocal fluorescence images. By simultaneously recording the absolute arrival-time of photons and the position information of piezo-electric translation stage with TTTR-TCSPC data acquisition card, the single-photon events and two-photon events for every pixel are counted synchronously during the scanning image. Figures 3(a) and 3(b) show the original intensity images of single-photon events and two-photon events, respectively. The bright spots in images represent single QDs or QD clusters. There is only a fraction of the spots appears in Fig. 3(b), which are mainly due to the heterogeneous multi-exciton emission of single QDs or the clusters with different QD number. Figure 3(c) shows a gated two-photon detection image, which is obtained by excluding the multi-exciton photons with GDT of 8 ns. These typical bright spots are marked by the letters from A to E in Figs. 3(a)-3(c). In Fig. 3(c), a lot of two-photon events are still in C and E, while few two-photon events are detected in A, B and D. In order to make the recognition more accurate, we remove the low-counting states caused by the weak excitation (QDs are not in the central position of laser

Optics EXPRESS

excitation) in focal imaging by plotting the PL intensity trace as a function of pixel for all pixels of every bright spot. Figure 3(d) shows a typical PL intensity trace at spot C. With a threshold of 30 counts/ms, the low-counting states are removed (see Appendix B for details). For the low-counting states, the proportion of background becomes larger and the impact of shot noise also becomes larger. Therefore, removing the low-counting states will make the recognition more accurate. Furthermore, we make the correction for the cross-talk between detectors, background and dark counts (see Appendix C for details). By using the modified photons, the various values obtained are used to calculate the number n of QDs for spots from A to E, as shown in Table 1. The calculated n with corresponding values of f_1 and f_2 are shown in Fig. 3(e). C and E further deviate from the black line of n = 1 and thus are recognized as QD clusters. A, B, D and the other spots approach the black line of n = 1 and thus are recognized as single QDs. The black error bars for all n values in Fig. 3(e) represent the impacts of shot noise. By calculating the n for all of the isolated bright spots in the image, the distribution of n can be obtained as shown in Fig. 3(f). The cyan and yellow circles marked with 1 and 2 represent single QDs and QD clusters, respectively. At last, the viability of the recognition is also assessed by the time-gated antibunching technique (see Appendix D for details).

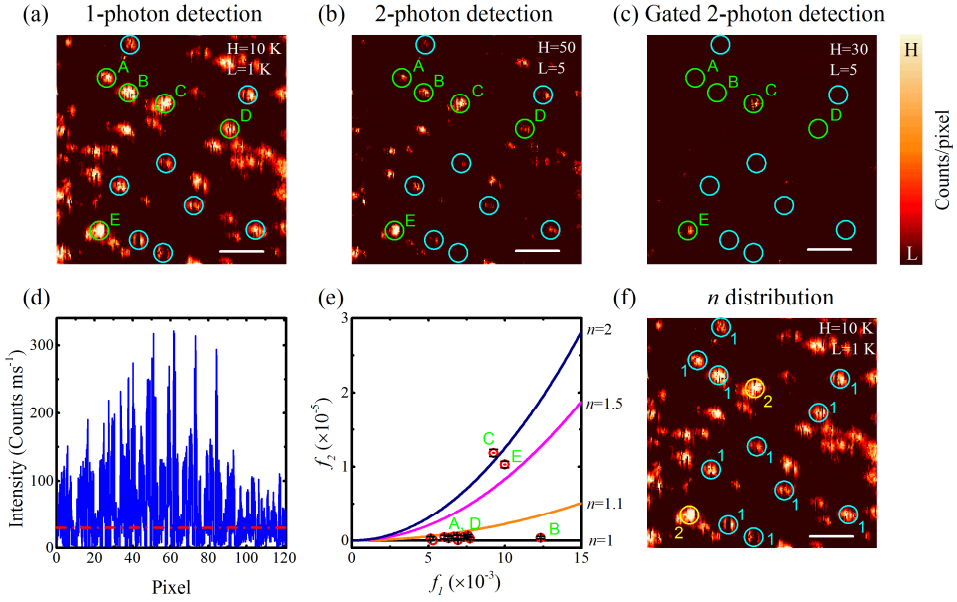

Fig. 3. Fast recognition the number n of QDs during confocal scanning imaging. (a, b) Typical example of images of single- and two-photon detection events of QDs on a glass coverslip. (c) Gated two-photon detection events of QDs extracted from (b) with GDT of 8 ns. (d) PL intensity trace reconstructed by extracting arrival time of photons from all the pixels of bright spot C, and a threshold of 30 counts/ms is used to remove the low-counting state. (e) Calculated n with corresponding values of f_1 and f_2, for the spots marked by cyan and green circles in (a-c). (f) Distribution of the number n of QDs in the confocal image. The cyan and yellow circles marked with 1 and 2 represent for single QDs and QD clusters, respectively. H and L are the maximum and minimum values of the intensity scale, respectively. 200 × 200, 80 nm imaging pixels and scale bars of 3 μm. The pixel dwell time is 60 ms.

Optics EXPRESS

Table 1. The various values used for the calculation of the number *n* of QDs marked in Figs. 3(a)-3(c).

Serial	Sync pulses (M)	single-photon events	two-photon events	f_1 (× 10^{-3})	f_2 (× 10^{-6})	*n*
A	35.58	246761	2	6.94	0.05	1.004
B	56.41	695952	21	12.34	0.37	1.01
C	54.87	508310	650	9.26	11.85	2.23
D	38.27	295535	9	7.72	0.25	1.017
E	58.77	587377	606	9.99	10.31	1.7

This method is considered to be fast because the single QDs can be recognized synchronously by using the collected photons during the scanning process. The dwell time at each pixel is 60 ms for our confocal system, and the recognition time is mainly limited by the homemade confocal scanning microscope with a piezo-scan stage. We recommend using at least 6000 photons (after time-gated) to do the recognition. The fewer photons will cause the larger shot noise which makes the recognition inaccurate (see Appendix C for details). If the quantum yield of QDs is high, the fast recognition can be achieved with the sufficient photons obtained in a short time.

5. Summary

We have demonstrated a new method to successfully recognize single QDs from high multi-exciton emission and clustering effects. By the TTTR-TCSPC technique, the effect of multi-exciton on recognition of single QDs could be removed effectively to satisfy the assumption-I of the spatial coincidence-counting model. By using the modified photons to calculate the probabilities of detecting single-photon events and two-photon events per excitation pulse, the single QDs could be fastly recognized based on the spatial coincidence-counting model. The recognition accuracy has also been further improved by removing the background of low-counting state. For non-blinking QDs with high multi-exciton emission, the method can also be used as a powerful tool to distinguish the QD number in clusters. This method for fast recognition of single QDs by using the collected photons during the scanning process in confocal imaging is pre-requisite for the relevant studies of single-particle spectroscopy.

Appendix A: Sample preparation and experiment setup

The CdSe/ZnS alloyed QDs were ordered from Suzhou Xingshuo Nanotech Company (the PL emission peak is at ~615 nm; quantum yield is about 80%) and the QDs have a high multi-exciton emission (see the $g^{(2)}$ in Fig. 6(a)) and a great PL blinking. The BX quantum yield of the QDs is evaluated to be ~0.06 at low excitation power. However, the QDs with the high multi-exciton emission under an appropriate excitation are suitable to test our method. QDs in toluene with a concentration of 10^{-10}~10^{-9} mol/L was spin-coated onto a cleaned glass coverslip (Ted Pella) at a rotational speed of 3000 rpm.

This sample was excited by 485 nm pulse laser (PDL808, PicoQuant, 90 ps) with a repetition rate of 10 MHz. An oil immersion objective (Olympus, 100×, 1.3 NA) was used to focus laser light onto the sample and collect fluorescence simultaneously. The excitation power used for the experiments is ~251 W/cm^2, and the average number of photons absorbed per QD per pulse is estimated to be ~0.6 [11]. Under this excitation power, the radiative photons are enough for the recognition of single QDs. A piezo-scan stage (Tritor 200/20 SG) with an active x-y-z feedback loop mounted on the inversion microscope was used to scan the sample over the focused excitation spot. The fluorescence, passing through a dichroic mirror (Semrock) and a high pass filter (Semrock), was focused into a 100 μm pinhole to reject out-of-focus photons. After the pinhole, the fluorescence photons were split by a 50/50 beam splitter cube into two beams and finally detected by a pair of single-photon avalanche diode detectors (SPCM-AQR-15, PerkinElmer). The arrival time of every photon, as well as the synchronization of pulse laser, were recorded by a TTTR-TCSPC data acquisition card (HydraHarp 400, PicoQuant). With a routine written in MATLAB, we can get the PL intensity traces, decay curves, the probabilities of detecting single- and two-photon events,

Optics EXPRESS

and $g^{(2)}(\tau)$ curve simultaneously. All measurements were performed at room temperature. We recommend putting the beam splitter after lens to diffuse the photons emitted by single-photon detectors. By this way, the cross-talk between the two single-photon detectors can be greatly suppressed. However, a few cross-talk photons still be detected, the detecting probability of the cross-talk photons in our setup has been evaluated to correct the recognition, as shown in Appendix C.

Appendix B: The method for removing low-counting states

The low-counting states of focal images are caused by the weak excitation and PL blinking. For the low-counting states, the proportion of background noise becomes larger and the impact of shot noise also becomes larger. Therefore, an intensity threshold was employed to remove the low-counting states to make the recognition more accurate. Fig. 4(a) shows a typical PL intensity trace of single CdSe/ZnS alloyed QDs. An appropriate threshold based on the intensity histogram is set to separate the trace into two states: high-counting states and low-counting states. After removing the low-counting states, the high-counting states of the trace is shown in Fig. 4(b). By this way, we can remove the background noise in low-counting states. As previously mentioned in Section 2, the reduced background can improve the recognition accuracy to make the values of *n* further approach to be an integer. In Section 4, we use the similar method to improve the recognition accuracy of single QDs in confocal fluorescence imaging.

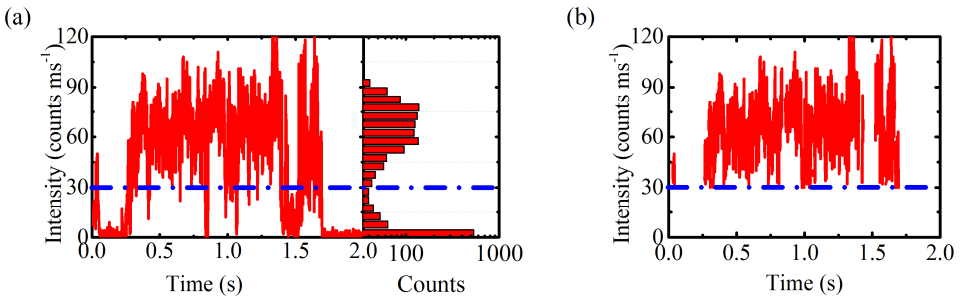

Fig. 4. (a) Typical PL intensity trace of single CdSe/ZnS alloyed QDs with a bin time of 1 ms, and the corresponding PL intensity histogram. The blue dash line is a threshold to separate the high-counting states and low-counting states. (b) The intensity trace with high-counting states.

Appendix C: The method for removing the effect of background noise

The background noise is mainly arising from background counts, dark counts, and cross-talk between detectors. The effects of background counts, dark counts, and cross-talk between detectors can be corrected by the following methods.

1) The total counts (N_{total}) recorded by detectors, can be expressed as

$$N_{total} = S + N_b + N_{cross} \pm \sqrt{N_{total}}, \tag{3}$$

where S , N_b , N_{cross} and $\sqrt{N_{total}}$ are the signal of QDs, background and dark counts, cross-talk between detectors and shot noise, respectively.

2) The two-photon events (or the coincidence counts) recorded by detectors, donated with N_c, can be expressed as

$$N_c = S_2 + \frac{1}{2}\frac{N_b}{Ft} N_{total} + N_{cross} \pm \sqrt{N_c}, \tag{4}$$

Optics EXPRESS

where S_2 is two-photon events originating from QD clusters and multi-exciton emission, F is the repetition rate of laser excitation, t is the total recording time.

3) The value of N_b can be determinate by the following method. A typical intensity trace of N_b is obtained under the same experimental conditions, as shown in Fig. 5(a). The corresponding decay curve of N_b is shown in Fig. 5(b). Based on the decay curve, the value of N_b as a function of GDT is shown in Fig. 5(c), so the values of N_b depend on the different GDTs. For a given GDT, the corresponding N_b is used as a corrected value.

4) The cross-talk between detectors can be expressed as $N_{cross} = \xi N_{total}$, where ξ is the probability of one detector detecting a cross-talk photon from another detector and can be estimated to be ~3.1 × 10^{-5} for our system. The details are as follows. For determining the impact of the cross-talk on the two-photon events, we have measured the $g^{(2)}$ for a background, as shown in Fig. 5(d). By comparing the area of the center and side peaks, the cross-talk is about 1789, and the total photons recorded by the two detectors is 57 M. Therefore, after a photon is detected by one detector, the probability of the other detector detecting a cross-talk photon is 3.1 × 10^{-5}.

5) The shot noise mainly affects the detecting two-photon events. For the fewer total photons, the impact of shot noise on the recognition of single QDs would become larger. The effect of shot noise on n is ~ ± 0.02 for the total photons of 300 K (after time-gated), while the effect of shot noise on n is ~ ± 0.1 for the total photons of 6 K (after time-gated).

At last, by substituting the values of N_{total}, N_c, $N_{b,}$ and N_{cross} into Eqs. (3) and (4), S and S_2 can be calculated as single- and two-photon events, respectively. After that, the probability of detecting a single- and two-photon events after an excitation pulse, donated with f_1 and f_2, can be calculated as $f_1 = S / Ft$ and $f_2 = S_2 / Ft$, respectively. The corrected f_1 and f_2 are used to calculate the number of QDs to make the recognition more accurate.

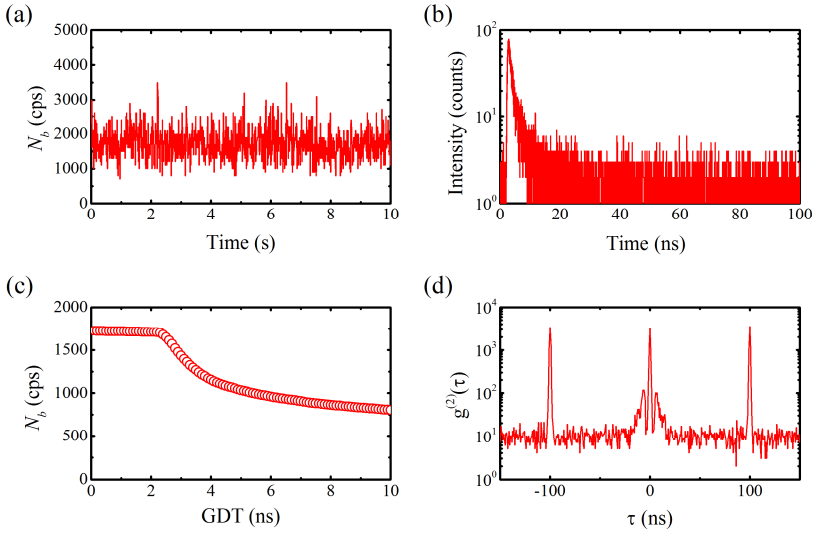

Fig. 5. (a) Typical intensity trace of background and dark counts (N_b). (b) The corresponding decay curve of N_b. (c) N_b as a function of GDT. (d) The second-order correlation function of N_b.

Optics EXPRESS

Appendix D: Assessing the viability of the method by the time-gated antibunching technique

A typical $g^{(2)}(\tau)$ with $g^{(2)}(0)$ of 0.68 for single CdSe/ZnS alloyed QDs is shown in Fig. 6(a). We define R_{TG} as the area ratio between the central and side peak in time-gated $g^{(2)}(\tau)$. By using the time-gated antibunching technique, we can get the values of R_{TG} as a function of GDT as shown in Fig. 6(b) with the red curve. The value of R_{TG} decreases very fast from 2.4 ns to 4.0 ns which correspond to the decay curve of multi-exciton state in Fig. 2(b). Finally, with the equation of $R_{TG} = (n\text{-}1)/n$ [12], the number n as a function of GDT can be represented by the blue curve as shown in Fig. 6(b). The result is in agreement with the red curve in Fig. 2(c). With the GDT of 8 ns, the time-gated $g^{(2)}(\tau)$ with a fairly small zero-time delay peak is shown in Fig. 6(c), which provides a clear evidence of single QD. It also demonstrates the viability of our method.

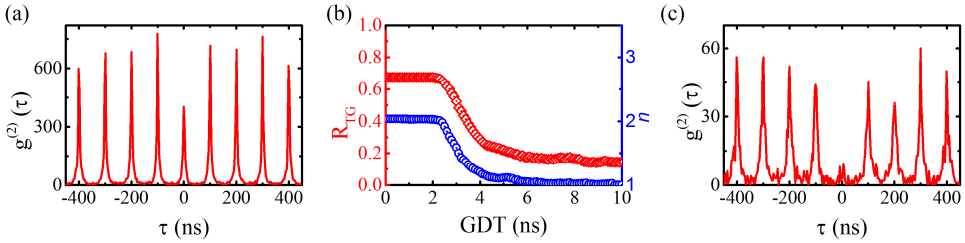

Fig. 6. (a) Typical second-order correlation function, $g^{(2)}(\tau)$, of single CdSe/ZnS alloyed QDs with $g^{(2)}(0)$ of 0.68. (b) Red squares: the ratio of the central and side peak (R_{TG}) of $g^{(2)}(\tau)$ function as a function of GDT. Blue circles: the calculated number n of QDs as a function of GDT. (c) $g^{(2)}(\tau)$ plot after GDT of 8 ns.

In addition, the second-order correlation function and time-gated second-order correlation function with GDT of 8 ns for spots A-E are shown in Figs. 7 (a)-7(e). The gray line is the original second-order correlation function, and the red line is the time-gated second-order correlation function with GDT of 8 ns. It is shown that the center peaks still exist for spots C and E with GDT of 8 ns while the other center peaks decay to zero for the other spots with GDT of 8 ns.

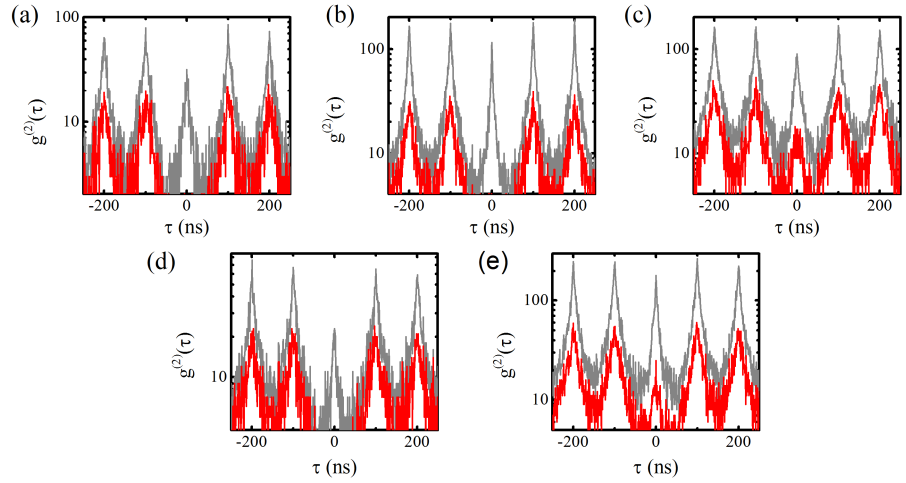

Fig. 7. The original second-order correlation function curves (black) and time-gated second-order correlation function curves with GDT of 8 ns (red) for spots A-E (a-e).

Optics EXPRESS

Appendix E: The lifetime distribution of single QDs and the recognition with a repetition rate of 5 MHz

We have measured the decay curves for ~100 single QDs with a lower repetition rate of 5 MHz. The histogram of the SX lifetime values is shown in the Fig. 8(a), and ~25 ns is the largest lifetime value which is approximately one-fourth of the pulse period of 100 ns (10 MHz). Therefore, the repetition rate of 10 MHz in work should be enough for the lifetime measurement.

We have also recognized the single QDs by our method with the repetition rate of both 5 MHz and 10 MHz, and it is found that the repetition rates don't affect the recognition of single QDs. As shown in Fig. 8(b), the calculated *n* of single QD is ~1 with GDT of 8 ns at 10 MHz, while the calculated *n* for the same single QD also is ~1 with GDT of 8 ns at 5 MHz. Therefore, the calculated *n* for the same QD is same with GDT of 8 ns at 5 MHz and 10 MHz. This is because the multi-exciton photons can be removed with an appropriate GDT. Though there are different values at GDT of 0 ns, which implies more multi-exciton photons at 10 MHz. But the more multi-exciton photons do not affect the recognition of single QDs. In addition, the more photons are easy to be obtained at a given time with the repetition rate of 10 MHz to make the recognition more accurate.

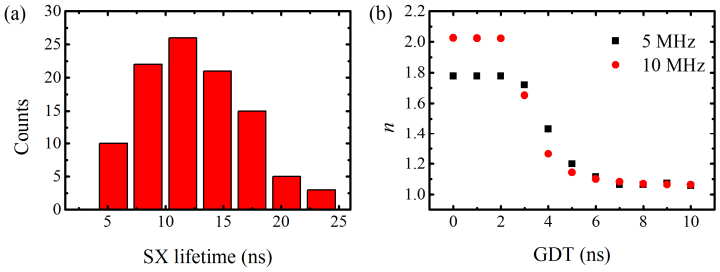

Fig. 8. (a) The histogram of the SX lifetime values. (b) Calculated *n* as a function of GDT for the same single QD measured at 5 MHz and 10 MHz.

Appendix F: The relationship between the first-photon emission and the calculated *n*

Here, we discuss the relationship between the first-photon emission presented in Fig. 2(b) and the *n* in Fig. 2(c). The cumulative distribution function (CDF) of the first-photon emission trace is calculated as shown in Fig. 9. It is found that the CDF starts at 1 and decreases with the integral of the normalized counts until it reaches 0, and the CDF completely overlaps with the trace of calculated number *n*. There is a good agreement between the CDF and *n*.

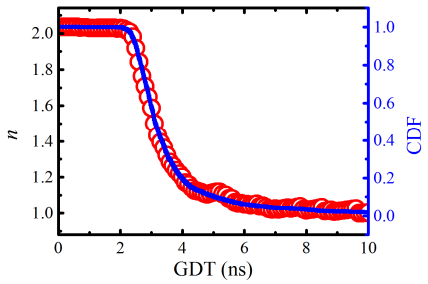

Fig. 9. Red circles: the calculated number *n* of emitters as a function of GDT. Blue curve: the calculated CDF of the first-photon emission.

Optics EXPRESS

Funding

National Key R&D Program of China (No. 2017YFA0304203), Natural Science Foundation of China (Nos. 61527824, 61675119, U1510133, 11434007, 11504216, 61605104), PCSIRT (No. IRT13076), 1331KSC, and Fund Program for the Scientific Activities of Selected Returned Overseas Professionals in Shanxi Province.